ICAS 2016
30th Congress of the International Council of the Aeronautical Sciences
DCC, Daejeon, Korea ; September 25-30, 2016

# ADAPTIVE SLIDING MODE CONTROLLER DESIGN FOR RECONFIGURATION OF ORGANIC FLIGHT ARRAY

**Junho Jeong, Seungkeun Kim, Jinyoung Suk**
**Chungnam National University, Republic of Korea**

**Keywords**: *Flight Array, Ducted-fan, Adaptive Sliding Mode Control*

## Abstract

*This paper presents an attitude control system for an organic flight array(OFA) which is a novel unmanned aerial vehicle(UAV) concept to consist of multiple ducted-fan UAVs. The OFA is able to be assembled or separated by single modules, the ducted-fan UAVs, to fulfill operation missions such as indoor/outdoor monitoring, communication relay, and system jamming. Therefore, the array can have various configurations depending on purposes of operation or environment. Physical parameters of the OFA change during the mission according to the reconfigurable feature, which generates dynamic uncertainties. Moreover, there might be an interactive effect due to connection between the ducted-fan modules. To cope with these uncertainties, a sliding mode control technique is used with applying an adaptive law in this paper. In addition, the performance of the designed controller is verified via numerical simulation.*

## 1 Introduction

Recently, there have been several studies on connecting platforms based on unmanned systems for aerial applications: a redundant actuation system[1], transporting payloads[2], and a distributed flight array(DFA)[3]. The DFA is connected by single-rotor individual modules, and consists of frame and docking mechanism, drive unit, flight unit, and electronic devices for operation. This array, however, cannot fly independently due to uncontrollable nature of the single module. This study proposes an organic flight array(OFA) consisted of multiple ducted-fan UAVs differently from the abovementioned works to improve applicability of the array system, since the ducted-fan UAV can fly by itself and has a duct-shape exterior structure which can easily accommodate a connecting equipment for assembly or separation. The proposed array is able to assemble and separate with regard to missions on the ground or the air. Figure 1 shows an operation concept of the OFA system[4]. This array is also classified as a reconfigured system. Therefore, dynamic characteristics of the array might be changed with unpredictable effects as dynamic uncertainties, when the configuration is rearranged during its mission. To cope with dynamic uncertainties, adaptive laws for VTOL(vertical take-off and landing) UAVs have been studied[5-6]. An adaptive sliding mode control technique was proposed for a quadrotor system to estimate dynamic error by sensor noise and ground effects during landing[5]. Also, a neural-network adaptive control was applied for a small ducted-fan UAV, GTSpy, to compensate inversion errors[6]. Moreover, an interacting effect was investigated for a ducted-fan aerial vehicle(DFAV) in [7]. It derived dynamic modeling of the DFAV and the interaction effect with horizontal and vertical fixed surfaces, and dealt with controlling problem.

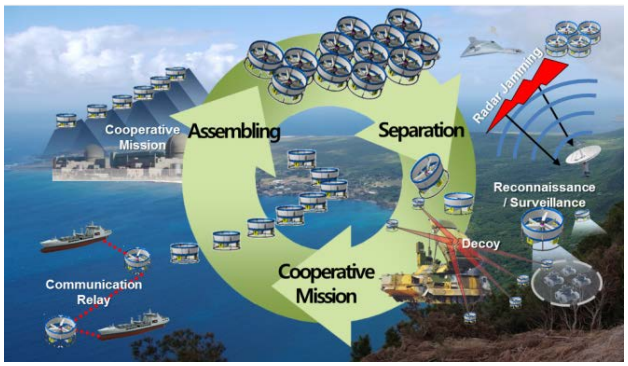


**Fig. 1. Operation Concept of the OFA[4]**

This study proposes the flight array system based on the ducted-fan UAVs. Also, an adaptive sliding mode controller is designed to overcome the dynamic uncertainties due to the reconfigurable feature. Moreover, the performance of the controller is verified via numerical simulation by using a derived numerical modeling to consider dynamic characteristics of the OFA.

This paper is organized as follows. Section 2 presents the dynamic modeling of the OFA. The attitude control system, based on the sliding mode control method with the adaptive law to overcome model uncertainties, is discussed in Section 3. Also, Section 4 shows simulation results under a reconfiguration scenario. Finally, Section 5 concludes this paper.

## 2 Dynamic Modeling

The dynamic modeling of the organic flight array is presented in this section. The OFA is constructed with multi ducted-fan modules and has a changeable configuration by assembly or separation. In order to take the abovementioned features into account, the numerical model is composed of the three parts: ducted-fan dynamics, geometric, and interacting effects.

Equations of motion are derived by six degrees of freedom with forces and moments based on a body frame of the array as follows:

$$\begin{aligned} \dot{u} &= vr - wq + F_x / m_o \\ \dot{v} &= wp - ur + F_y / m_o \\ \dot{w} &= uq - vp + F_z / m_o \end{aligned} \tag{1}$$

$$\begin{aligned} \dot{p} &= \{qr(J_{o,yy} - J_{o,zz}) + M_x\} / J_{o,xx} \\ \dot{q} &= \{pr(J_{o,zz} - J_{o,xx}) + M_y\} / J_{o,yy} \\ \dot{r} &= \{pq(J_{o,xx} - J_{o,yy}) + M_z\} / J_{o,zz} \end{aligned} \tag{2}$$

where $(u,v,w)$ and $(p,q,r)$ indicate velocities and angular rates on each axis, respectively. $m_o$ and $J_o$ represent mass and moment of inertia of the OFA. Moreover, the forces $(F)$ and moments $(M)$ consist of the ducted-fan, the geometric, and the interaction effects. In addition, Euler rates $(\dot{\phi},\dot{\theta},\dot{\psi})$ are defined in terms of Euler angles $(\phi,\theta,\psi)$ and the body angular velocities as

$$\begin{aligned} \dot{\phi} &= p + qS_\phi T_\theta + rC_\phi T_\theta \\ \dot{\theta} &= qC_\phi - rS_\phi \\ \dot{\psi} &= \left(qS_\phi + rC_\phi\right)/C_\theta \end{aligned} \tag{3}$$

where Eq. (3) uses shorthand notations as $C_\phi \equiv \cos\phi$, $S_\phi \equiv \sin\phi$, and $T_\theta \equiv \tan\theta$.

### 2.1 Ducted-fan Module

A coordinate system of the single ducted-fan module is defined as shown in Fig.2. The forces and moments of the ducted-fan module are

$$\begin{aligned} F_{total_i} &= F_{fuse_i} + F_{rotor_i} + F_{duct_i} + F_{flap_i} + F_{grav_i} \\ M_{total_i} &= M_{fuse_i} + M_{rotor_i} + M_{duct_i} + M_{flap_i} + M_{gyro_i} \end{aligned} \tag{4}$$

where the terms are derived for the $i$ th module. The terms consist of each component[6]: fuselage ( $fuse$) , rotor, duct, flap, gravitational forces ($grav$) , gyroscopic moments ($gyro$) .

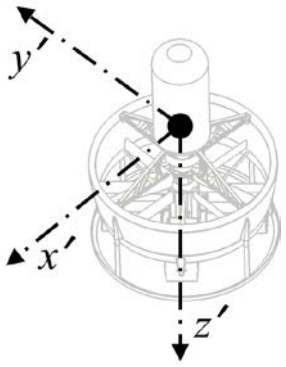


**Fig. 2. Coordinate System of the Ducted-fan Module**

These terms are referred to as derived equations in [6] except the rotor term due to avoidance of iterative calculation. Therefore, Simple rotor dynamics are applied in the study as follows:

$$F_{rotor} = \begin{bmatrix} 0 \\ 0 \\ -T \end{bmatrix}, \quad M_{rotor} = \begin{bmatrix} 0 \\ 0 \\ \tau \end{bmatrix} \tag{5}$$

where $T$ and $\tau$ represent thrust and torque, respectively. For the rotor dynamics, these elements can be calculated by DFDC(ducted-fan

design code) software[8] to input geometric data of the ducted-fan module. Moreover, an induced velocity ($v_{ind}$), to calculate the control power by the flaps, is obtained with respect to $RPM$ as follows:

$$\begin{aligned} T &= b_{thr,1}RPM + b_{thr,2}RPM^2 \\ \tau &= b_{tor,1}RPM + b_{tor,2}RPM^2 \\ v_{ind} &= b_{vel,1}RPM + b_{vel,2}RPM^2 + b_{vel,3}RPM^3 \end{aligned} \quad (6)$$

where the parameters are summarized in Table 1.

**Table 1. Parameters of the Rotor Model**

| Component | $b_{com,1}$ | $b_{com,2}$ | $b_{com,3}$ |
|---|---|---|---|
| *thr* | *-1.56e-3* | *4.14e-6* | - |
| *tor* | *9.03e5* | *-2.69e-8* | - |
| *vel* | *1.72e-3* | *7.57e-7* | *-7.27e-11* |

Then forces and moments of the $i$ th module can be arranged as

$$F_{total_i} = \begin{bmatrix} F_{x_i} \\ F_{y_i} \\ F_{z_i} \end{bmatrix}, \quad M_{total_i} = \begin{bmatrix} M_{x_i} \\ M_{y_i} \\ M_{z_i} \end{bmatrix}. \quad (7)$$

The control flaps are defined by combinations of each flap: 1 and 3 are ailerons, 2 and 4 are elevators, and deflecting all of the flaps are rudders as described in Fig. 3 and Table 2. Each flap has deflection limits from -30 to +30 degrees[9]. Therefore each combination should be moved within these limitation angles. Then deflection angles of the combinations are limited from -15 to +15 degrees.

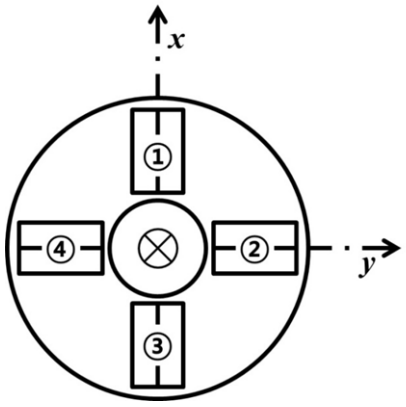


**Fig. 3. Definition of Control Flaps at Bottom View[9]**

**Table 2. Sing Conventions of Control Flaps[9]**

| No. of Flaps | Deflection | Sense | Effect |
|---|---|---|---|
| ①,③ | trailing edge left | $+\delta a$ | $+L$ |
| ②,④ | trailing edge down | $+\delta e$ | $+M$ |
| ①,②,③,④ | trailing edge counterclockwise | $+\delta r$ | $+N$ |

## 2.2 Geometric Effect

This effect is generated by the changeable configuration feature of the OFA due to not only change of the center of gravity, but also added force and moment terms. For instance, a new coordinate system of the OFA can be shown as Fig. 4 when it is constructed by four modules.

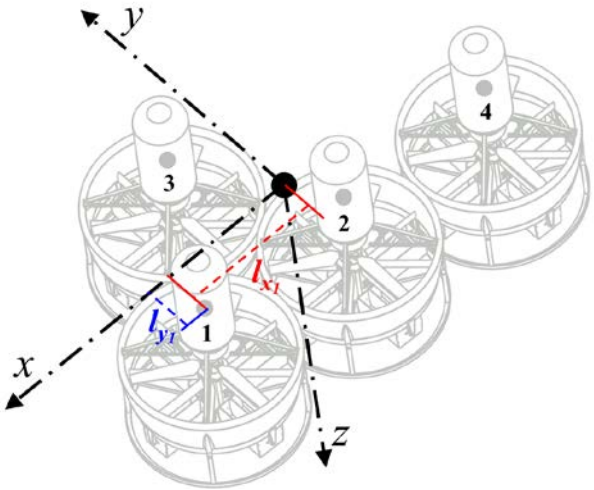


**Fig. 4. Coordinate System of the OFA**

In order to consider the geometric information with the module dynamics defined in Eq. (7), the forces and moments are given as follows:

$$F_x = \sum_{i=1}^{N} F_{x_i}, \quad F_y = \sum_{i=1}^{N} F_{y_i}, \quad F_z = \sum_{i=1}^{N} F_{z_i} \quad (8)$$

$$\begin{aligned} M_x &= \sum_{i=1}^{N} \left( M_{x_i} - l_{z_i} F_{y_i} + l_{y_i} F_{z_i} \right) \\ M_y &= \sum_{i=1}^{N} \left( M_{y_i} - l_{x_i} F_{z_i} + l_{z_i} F_{x_i} \right) \\ M_z &= \sum_{i=1}^{N} \left( M_{z_i} - l_{y_i} F_{x_i} + l_{x_i} F_{y_i} \right) \end{aligned} \quad (9)$$

where $l_{x,i}$ , $l_{y,i}$ , and $l_{z,i}$ indicate distances between the center of gravity of the flight array and the $i$ th ducted-fan. In this study, let us assume that the array is assembled on the same $x-y$ plane. Then $l_{z,i}$ can be neglected.

### 2.3 Interaction

Unpredictable dynamic terms might be incurred due to the changeable feature of the OFA during the flight mission. Contact forces, called as the interacting effect, is considered in this study. When a ducted-fan module is going to assemble with the array in the air, the contact forces are generated at the contact point between the added module and the array system with respect to relative angles $(\alpha, \beta, \gamma)$ shown in Fig. 5.

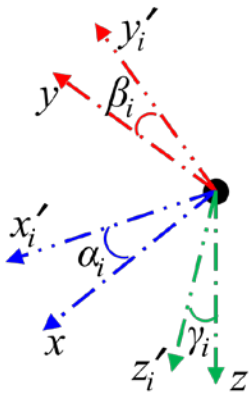


**Fig. 5. Relative Angles between the OFA and the *i*th Added Module at the Contact Time**

Then, the contact forces can be defined by accelerations of the $i$ th added module with a rotation matrix $(R)$ as follows:

$$\begin{bmatrix} F_{I,x} \\ F_{I,y} \\ F_{I,z} \end{bmatrix} = R \begin{bmatrix} \dot{u}_i m_i \\ \dot{v}_i m_i \\ \dot{w}_i m_i \end{bmatrix} \tag{10}$$

where the rotation matrix is

$$R = \begin{bmatrix} C_\beta C_\gamma & S_\alpha S_\beta C_\gamma - C_\alpha S_\gamma & C_\alpha S_\beta C_\gamma + S_\alpha S_\gamma \\ C_\beta S_\gamma & S_\alpha S_\beta S_\gamma + C_\alpha C_\gamma & C_\alpha S_\beta S_\gamma - S_\beta C_\gamma \\ -S_\beta & S_\alpha C_\beta & C_\alpha C_\beta \end{bmatrix}.$$

Moreover, moments are derived as

$$\begin{bmatrix} M_{I,x} \\ M_{I,y} \\ M_{I,z} \end{bmatrix} = \begin{bmatrix} d_y F_{I,z} - d_z F_{I,y} \\ d_z F_{I,x} - d_x F_{I,z} \\ d_x F_{I,y} - d_y F_{I,x} \end{bmatrix} \tag{11}$$

where $d_x$ , $d_y$ , and $d_z$ represent distances between the center of gravity of the OFA and the contact point.

## 3 Attitude Controller

This section presents the attitude controller, which is designed by the adaptive sliding mode controller to cope with the model uncertainties. To design this controller, affine systems are rearranged from the derived model. Then, the adaptive law is derived to overcome dynamic uncertainties due to the reconfigurable feature by the added module. Let us assume that the flaps are only used for the attitude control to simplify an allocation problem in this study, although the OFA can be controlled by both the flap and the RPM inputs.

### 3.1 Affine System

For the attitude dynamics, control-affine form is divided into two affine systems with respect to response speed: fast and slow dynamics. The derived equations, in Section 2, are rewritten as the affine form as follows:

$$\dot{x}_j = f_j(x) + g_j(x)u_j + \upsilon_j \tag{12}$$

where $j$ is an index to distinguish between the slow $(j=1)$ and fast $(j=2)$ dynamics. $\upsilon_j$ indicates dynamic uncertainties. This uncertain term is only considered in the fast dynamics, since the slow dynamics is composed of relation between the Euler rates and the body angular velocities as Eq. (3).

#### *3.1.1 Slow Dynamics*

State and input vectors of the slow dynamics are $x_1 = [\phi, \theta, \psi]^T$ and $u_1 = [p, q, r]^T$ , respectively. Then, the affine system of the slow dynamics is defined as follows:

$$\dot{x}_1 = f_1(x) + g_1(x)u_1 \tag{13}$$

$$f_1 = \begin{bmatrix} 0 \\ 0 \\ 0 \end{bmatrix}$$
$$g_1 = \begin{bmatrix} 1 & S_\phi T_\theta & C_\phi T_\theta \\ 0 & C_\phi & -S_\phi \\ 0 & S_\phi / C_\theta & C_\phi / C_\theta \end{bmatrix} \quad (14)$$

where $g_1(x)$ is invertible during the general operation of the OFA. In addition, the slow dynamics has no uncertain model $\upsilon_1$ in this study.

### *3.1.2 Fast Dynamics*

The affine system of the fast dynamics is

$$\dot{x}_2 = f_2(x) + g_2(x)u_2 + \upsilon_2 \quad (15)$$

where $x_2 = [p, q, r]^T$ and input vector is $u_2 = [\delta a_1, \delta e_1, \delta r_1, \cdots, \delta a_N, \delta e_N, \delta r_N]^T$. The size of the input vector is changed with respect to the number of the single modules $(N)$. Then the dynamic elements are rewritten as follows:

$$f_2 = \begin{bmatrix} \{qr(J_{o,yy} - J_{o,zz}) + L_a\} / J_{o,xx} \\ \{pr(J_{o,zz} - J_{o,xx}) + M_a\} / J_{o,yy} \\ \{pq(J_{o,xx} - J_{o,yy}) + N_a\} / J_{o,zz} \end{bmatrix} \quad (16)$$

where

$$X_a = \sum_{i=1}^{N} \left( F_{fuse,x_i} + F_{duct,x_i} + F_{grav,x_i} \right)$$
$$Y_a = \sum_{i=1}^{N} \left( F_{fuse,y_i} + F_{duct,y_i} + F_{grav,y_i} \right)$$
$$Z_a = \sum_{i=1}^{N} \left( F_{fuse,z_i} + F_{duct,z_i} + F_{grav,z_i} + F_{rotor,z_i} \right)$$
$$L_a = \sum_{i=1}^{N} \left( M_{fuse,x_i} + M_{duct,x_i} + M_{gyro,x_i} - l_{z_i} Y_{a_i} + l_{y_i} Z_{a_i} \right)$$
$$M_a = \sum_{i=1}^{N} \left( M_{fuse,y_i} + M_{duct,y_i} + M_{gyro,y_i} - l_{x_i} Z_{a_i} + l_{z_i} X_{a_i} \right)$$
$$N_a = \sum_{i=1}^{N} \left( M_{rotor,z_i} - l_{y_i} X_{a_i} + l_{x_i} Y_{a_i} \right).$$

$$G_2(x,u) = \begin{bmatrix} L_b / J_{o,xx} \\ M_b / J_{o,yy} \\ N_b / J_{o,zz} \end{bmatrix} \quad (17)$$

where

$$X_b = \sum_{i=1}^{N} F_{flap,x_i}, \quad Y_b = \sum_{i=1}^{N} F_{flap,y_i}$$
$$L_b = \sum_{i=1}^{N} \left( M_{flap,x_i} - l_{z_i} \cancel{Y_{b_i}} \right)$$
$$M_b = \sum_{i=1}^{N} \left( M_{flap,y_i} + l_{z_i} \cancel{X_{b_i}} \right)$$
$$N_b = \sum_{i=1}^{N} \left( M_{flap,z_i} - l_{y_i} X_{b_i} + l_{x_i} Y_{b_i} \right)$$

, and assume that $l_{z,i}$ is neglected. Then $g_2(x)$ is derived from Eq. (17) as

$$g_2 = \begin{bmatrix} G_2(1,1) & 0 & 0 & \cdots \\ 0 & G_2(2,2) & 0 & \cdots \\ G_2(3,1) & G_2(3,2) & G_2(3,3) & \cdots \end{bmatrix} \quad (18)$$

where

$$G_2(1, 4(i-1)+1) = \text{sgn}(v_{ind} - w) \kappa_{ail,i} l_{ail} / J_{o,xx}$$
$$G_2(2, 4(i-1)+2) = \text{sgn}(v_{ind} - w) \kappa_{ele,i} l_{ele} / J_{o,yy}$$
$$G_2(3, 4(i-1)+1) = -l_{x_i} \text{sgn}(v_{ind} - w) \kappa_{ail,i} / J_{o,zz}$$
$$G_2(3, 4(i-1)+2) = -l_{y_i} \text{sgn}(v_{ind} - w) \kappa_{ele,i} / J_{o,zz}$$
$$G_2(3, 4(i-1)+3) = \text{sgn}(v_{ind} - w) \kappa_{rud,i} l_{rud} / J_{o,zz}$$
$$\kappa_{flap,i} = q_{flap} C_{L_{\delta flap}} S_{flap}$$

where $q_{flap}$, $C_{L_{\delta flap}}$, $S_{flap}$, and $l_{flap}$ represent dynamic pressure, lift coefficient, area, and moment arm of each combination of the flaps: aileron $(\delta a)$, elevator $(\delta e)$, and rudder $(\delta r)$. Moreover, the size of $g_2(x)$ matrix is expanded with respect to the number of the ducted-fan modules as $g_2(x) \in \Re^{3 \times 4N}$. The uncertain model $\upsilon_2$ contains the interacting effects which is derived in Eqs. (10) and (11). Also, this model includes geometric uncertainties due to reconfiguration by aerial connection situation: the change of the center of gravity and the moment of inertia, inaccurate position and weight information of the added module.

## 3.2 Sliding Mode Control

The attitude controller is designed based on sliding mode control method for the fast and the slow dynamics. An outer loop of the control system applies a pure sliding mode control law for the slow dynamics. Moreover, the adaptive law is considered to cope with the model

uncertainties in an inner loop for the fast dynamics. This attitude control system is constructed as shown in Fig. 6.

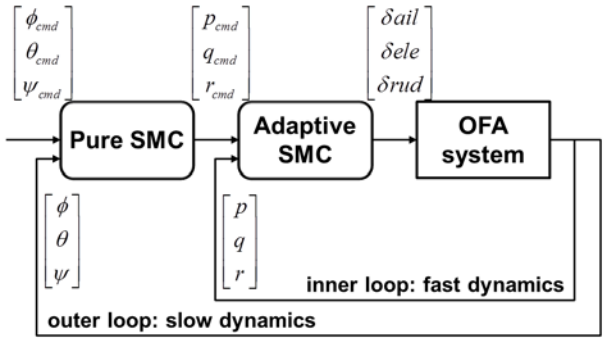


**Fig. 6. Attitude Control System**

In order to design the controller, a sliding surface is defined as

$$S_j = e_j \tag{19}$$

where $e_j = x_j - x_{j,cmd}$ is the state error vector of the fast and the slow dynamics. The states follows the commands, when the sliding surface converges to zero.

### *3.2.1 Pure SMC: Slow Dynamics*

For the slow dynamics, a Lyapunov candidate function is defined with the sliding surface as:

$$L_1 = \frac{1}{2} S_1^T S_1 \ . \tag{20}$$

Differentiating Eq. (20) with respect to time is derived as

$$\begin{aligned} \dot{L}_1 &= S_1^T \dot{S}_1 \\ &= S_1^T \left[ \dot{x}_1 - \dot{x}_{1,cmd} \right] \\ &= S_1^T \left[ f_1 + g_1 u_1 - \dot{x}_{1,cmd} \right] . \end{aligned} \tag{21}$$

The pure sliding mode control law is designed as

$$u_1 = g_1^{-1} \left[ -f_1 + \dot{x}_{1,cmd} - K_1 \operatorname{sgn}(S_1) \right] \tag{22}$$

where $K_1$ is a gain matrix with positive values. Then substituting the designed control input into Eq. (21) gives

$$\dot{L}_1 = -K_1 \left\| S_1 \right\| < 0 \ . \tag{23}$$

### *3.2.2 Adaptive SMC: Fast Dynamics*

For the fast dynamics, a new Lyapunov candidate function is designed based on Eq. (20) with the uncertain model. However, as $\upsilon_2$ is unmeasurable, the estimated value of $\upsilon_2$ is defined as $\hat{\upsilon}_2$. Then, the Lyapunov candidate function with the sliding surface and the uncertain term is

$$L_2 = \frac{1}{2} S_2^T S_2 + \frac{1}{2} \tilde{\upsilon}_2^T \Gamma^{-1} \tilde{\upsilon}_2 \tag{24}$$

where $\tilde{\upsilon}_2 = \upsilon_2 - \hat{\upsilon}_2$, and $\Gamma^{-1}$ is a positive definite diagonal matrix. Then, differentiating Eq. (24) with respect to time yields

$$\begin{aligned} \dot{L}_2 &= S_2^T \dot{S}_2 + \tilde{\upsilon}_2^T \Gamma^{-1} \dot{\tilde{\upsilon}}_2 \\ &= S_2^T \left[ f_2 + g_2 u_2 + \upsilon_2 - \dot{x}_{1,cmd} \right] \\ &\quad + \tilde{\upsilon}_2^T \Gamma^{-1} \left( -\dot{\hat{\upsilon}}_2 \right) \end{aligned} \tag{25}$$

where $-\dot{\hat{\upsilon}}_2 \cong \dot{\tilde{\upsilon}}_2$. Then the following control law can be designed as

$$u_2 = g_2^{-1} \left[ -f_2 - \hat{\upsilon}_2 + \dot{x}_{2,cmd} - K_2 \operatorname{sgn}(S_2) \right] \tag{26}$$

where $K_2$ is a gain matrix with positive values. Then, Eq. (25) can be rewritten as

$$\dot{L}_2 = -K_2 \left\| S_2 \right\| + \tilde{\upsilon}_2^T \left( S_2 - \Gamma^{-1} \dot{\hat{\upsilon}}_2 \right) . \tag{27}$$

From Eq. (27), an updated function, which is also called the adaptive law, is derived as

$$\dot{\hat{\upsilon}}_2 = \Gamma S_2 \ . \tag{28}$$

Substituting the adaptive law into Eq. (27) yields

$$\dot{L}_2 = -K_2 \left\| S_2 \right\| < 0 \ . \tag{29}$$

The control laws are derived as Eqs. (22) and (26). These have sign function, and it might experience a chattering problem. In order to reduce this problem, each sign function is replaced with a saturation function:

$$sat(S_j) = \begin{cases} S_j, & if \left| S_j \right| \le 1 \\ \operatorname{sgn}\left( S_j \right), & else \end{cases} . \tag{30}$$

## 4 Numerical Simulation

In this section, the attitude control system is verified for the reconfiguration of the OFA. This control system, abbreviated as ASMC, uses the pure and the adaptive sliding mode controller for the slow and the fast dynamics, respectively. In order to compare the control system, SMC is simulated by using only the pure sliding mode method for both the inner and outer loops. This simulation takes the assembly scenario into account to compare performances between the ASMC and the SMC with the interaction and geometry uncertainties due to configuration change. This scenario considers the OFA which is composed of three single modules. Then, one more single module is going to connect to the existing array in the air. Therefore, the configuration of this OFA is changed from the three-module-based array to the four-module-based array as shown in Fig. 7. However, the attitude control system has limited information for the new connected module. Let us assume that the connected module has less weight: equivalent to 5% weight uncertainty. Moreover, the controller has no exact location information of the connected module. Also, the combination of the flaps for the connected module is retained as same manner as the three-module-based OFA. Furthermore, the geometry uncertainties exist as the center of gravity and the moment of inertia of the new OFA.

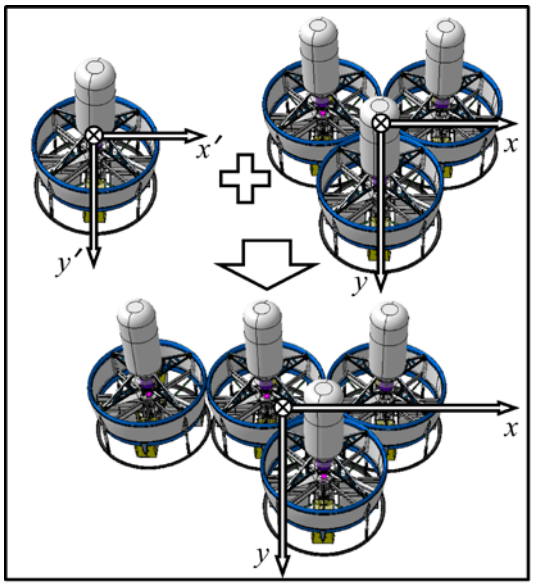


**Fig. 7. Description of the Simulation Situation**

Figures 8-10 show the comparison results for the reconfiguration simulation. The solid line represents the commands for each Euler angels in Fig. 8. The dash and the dash-dotted lines indicate the pure(SMC) and the adaptive(ASMC) sliding mode controller, respectively. The OFA is contacted by another ducted-fan module at 1 sec. Then the interacting forces are incurred by the time when these vehicles are completely connected at 2 sec. Let us assume that the interacting forces only generate on the x axis based on the connected module coordinates as follows:

$$F_{I,x}(t)=\begin{cases}1, & t=1\\ 1-(t-1), & 1\le t\le 2\\ 0, & else\end{cases}. \qquad (31)$$

Thus, the geometric uncertainties are incurred from 2 sec in this simulation. Figure 8 indicates the comparison results for the Euler angles, and Fig. 9 shows histories of the angular rates. The pure controller shows poor tracking performance with steady-state error to contrast the adaptive sliding mode controller, which means that the adaptation law compensates the model uncertainties effectively. Figure 10 shows the control inputs as averaging values by using Eq. (32) to improve legibility.

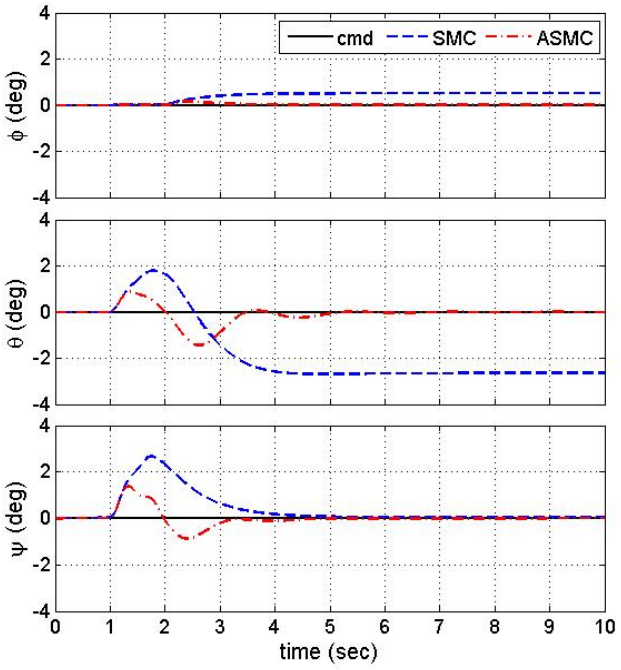


**Fig. 8. Trajectories of Euler Angles**

$$\delta a(t) = \frac{\sum_{1}^{N} \delta a_i(t)}{N}, \quad \delta e(t) = \frac{\sum_{1}^{N} \delta e_i(t)}{N} \qquad (32)$$
$$\delta r(t) = \frac{\sum_{1}^{N} \delta r_i(t)}{N} .$$

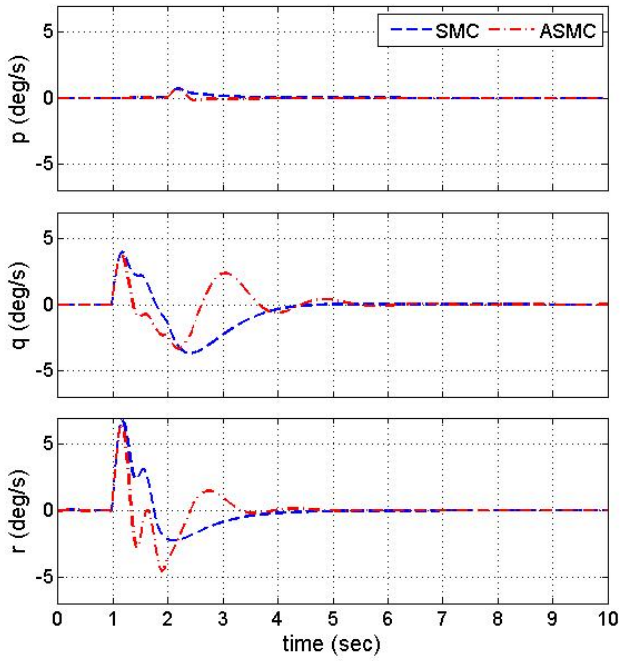


**Fig. 9. Trajectories of Angular Rates**

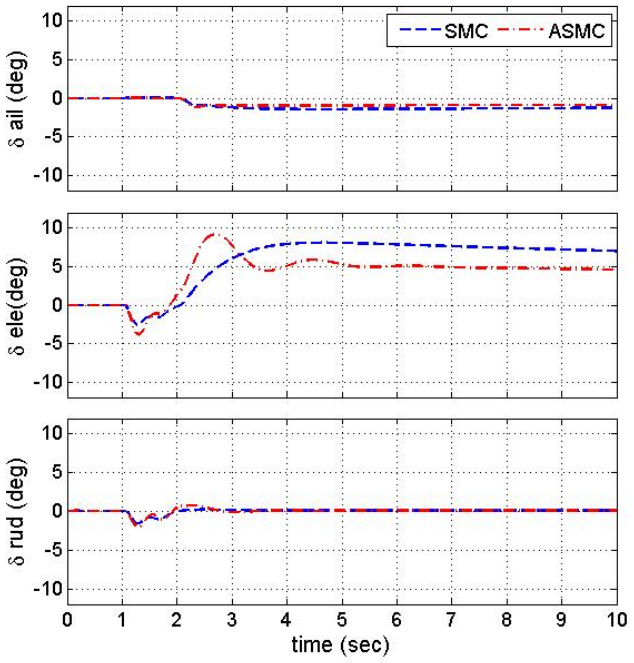


**Fig. 10. Trajectories of Average Inputs**

Also, Fig. 11 represents the estimates of the uncertainties $\hat{\upsilon}$. As shown in these trajectories, the adaptive law is properly designed to follow the dynamic uncertainties. Thus, this simulation verifies that the adaptive sliding mode controller is suitable for the reconfigurable flight array system.

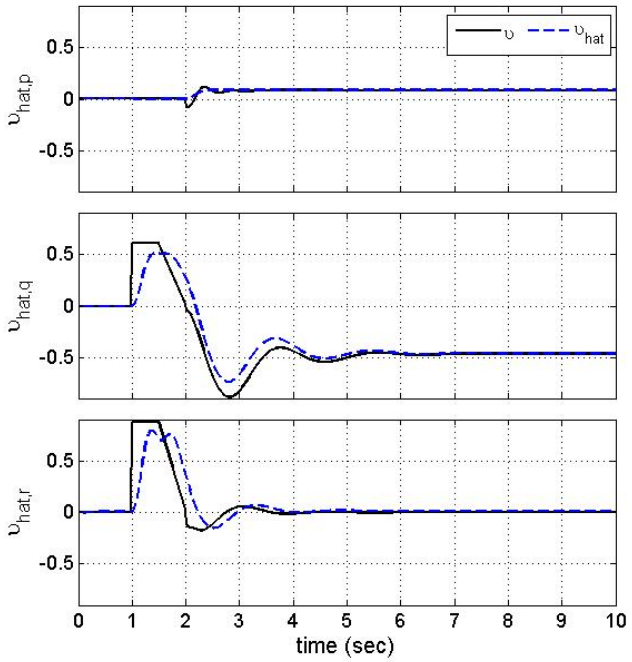


**Fig. 11. Trajectories of Estimation of Dynamic Uncertainties**

## 5 Conclusions

In this paper, the attitude controller was designed for the new-concept reconfigurable UAV, the organic flight array. The attitude control system was constructed by two dynamic modes: the slow and the fast dynamics. For the fast dynamics, the adaptive law was applied to compensate model uncertainties due to the reconfigurable feature. Moreover, the dynamic modeling of the proposed array was derived to consider the ducted-fan dynamics, the geometric, and the interacting effects with respect to configuration change by assembly or separation. Also, the numerical simulation was performed to take the assembly scenario into account. Then, the simulation results manifests the effectiveness and the feasibility of the attitude control system with the adaptation law for the reconfigurable flight array system.

## References

[1] R. Naldi, A. Ricco, A. Serrani, and L. Marconi, "A Modular Aerial Vehicle with Redundant Actuation," *Proc. 2013 IEEE/RSJ International Conference on Intelligent Robots and Systems*, Tokyo, Japan, 2013.

[2] D. Mellinger, M. Shomin, N. Michael, and V. Kumar, "Cooperative Grasping and Transport Using Multiple Quadrotors," *Springer Tracts in Advanced Robotics-Distributed Autonomous Robotic Systems: The 10th International Symposium*, Vol. 83, pp 545-558, 2013.

[3] R. Oung and R. D'Andrea, "The Distributed Flight Array," *Mechatronics*, Vol. 21, Issue 6, pp 908-917, 2011.

[4] B. Oh, J. Jeong, S. Kim, and J. Suk, "Design of Attitude Control System for Organic Flight Array based on Neural Network," *Proc. 7th Asia-Pacific International Symposium on Aerospace Technology*, Cairns, Australia, 2015.

[5] D. Lee, H. Kim, and S. Sastry, "Feedback Linearization vs. Adaptive Sliding Mode Control for a Quadrotor Helicopter," *International Journal of Control, Automation, and Systems*, Vol. 7, No. 3, pp 419-428, 2009.

[6] E.N. Johnson and M.A. Turbe, "Modeling, Control, and Flight Testing of a Small Ducted-Fan Aircraft," Journal of Guidance, Control, and Dynamics, Vol. 29, No. 4, pp 769-779, 2006.

[7] L. Gentili, R. Naldi, L. Marconi, "Modeling and Control of VTOL UAVs Interacting with the Environment," *Proc. 47th IEEE Conference on Decision and Control*, Cancun, Mexico, 2008.

[8] H. Youngren, M. Drela, and S. Sanders, *DFDC ver. 0.70*, Massachusetts Institute of Technology, Cambridge, MA, USA, 2005.

[9] J. Jeong, S. Kim, and J. Suk, "Control System Design for a Ducted-fan UAV using Linear Quadratic Tracker," *International Journal of Aerospace Engineering*, 2015.

## Contact Author Email Address

- Junho Jeong (mailto:junho@cnu.ac.kr)
- Seungkeun Kim (mailto:skim78@cnu.ac.kr)
- Jinyoung Suk (corresponding author, mailto:jsuk@cnu.ac.kr)

## Acknowledgment

This work was supported by Agency of Defense for Development (No. UD140062JD).

## Copyright Statement